Article

Not peer-reviewed version

Porous Europium Metal-Organic Frameworks as Highly Sensitive Bi-Functional Sensor for Isoprocarb and Levofloxacin

You Yin , Yuanhong Cheng , Ning Song * , Chenghui Zeng *

Posted Date: 25 May 2026

doi: 10.20944/preprints202605.1703.v1

Keywords: lanthanide MOFs; fluorescence; sensor; isoprocarb; levofloxacin

 doi:10.20944/preprints202605.1703.v1

Article

Porous Europium Metal-Organic Frameworks as Highly Sensitive Bi-Functional Sensor for Isoprocarb and Levofloxacin

You Yin [1], Yuanhong Cheng [2], Ning Song [3,*] and Chenghui Zeng [2,*]

[1] Medicing and Health Science College, Guangzhou Huashang College, Guangzhou, 511300, China
[2] National Engineering Research Center for Carbohydrate Synthesis, College of Chemistry and Materials, Jiangxi Normal University, Nanchang 330022, China
[3] Gannan Laboratory, Jiangxi University of Science and Technology, Ganzhou 341000, China
* Correspondence: 15147319329@163.com (N.S.); chenghuizeng@jxnu.edu.cn (C.Z)

Abstract

The development of highly sensitive fluorescence sensing materials has attracted much attention in recent years. In this study, a new two-dimensional porous europium metal-organic frameworks (**EuMOFs**) have been obtained. Studies have shown that **EuMOFs** is a stable, fast response, and highly sensitive fluorescence sensor for isoprocarb and levofloxacin (Lvx), which are closely related to food safety and human health. The limits of detection (LOD) for isoprocarb and Lvx are as low as 1.0 and 0.5 nM, respectively, which were much lower than the national standards (GB 28260-2011 for isoprocarb is 2.583 μM). **EuMOFs** can also achieve strong anti-interference detection of isoprocarb in apple peel and rice extract solution, and Lvx in real urine, with excellent detection stability in 0.01~9.0 nM. The recovery rates for isoprocarb and Lvx in real samples are in 99.12%~101.25%.

Keywords: lanthanide MOFs; fluorescence; sensor; isoprocarb; levofloxacin

1. Introduction

Isoprocarb can inhibit acetylcholinesterase, so they are widely used to kill insects. The use of pesticides improves crop yield and the preservation of agricultural products, but their residues also cause food and environmental pollution. The use of pesticides in cereals has been widely reported, and the trend of their use is expected to increase substantially in the coming decades, which is a serious concern. Isoprocarb that remains in plants, vegetables and fruits, can inhibit the activity of the human central and peripheral nervous system and lead to the accumulation of the neurotransmitter acetylcholine in the body, leading to acute poisoning. In addition, long-term intake of food with pesticide residue levels exceeding the recommended standards can lead to chronic poisoning, endocrine interference, reproductive impact, accelerate dementia, increase the risk of cancer [1]. The World Health Organization and the Food and Agriculture Organization of the United Nations have classified isoprocarb as a high-hazard pesticide. Therefore, the detection and quantitative analysis of isoprocarb is highly needed.

Levofloxacin (Lvx), as one of the fluoroquinolones, is a typical broad-spectrum antibiotics, which is widely used in the treatment of various bacterial infections in animals and humans, pharmaceutical, food, environment and other fields. Improper use of Lvx may cause adverse symptoms such as heart disease, central nervous system reactions, respiratory system damage, gastrointestinal damage, immune dysfunction, impaired kidney function, and lead to serious multi-antibiotic resistance, threatening global public health [2]. And excessive use of Lvx is not completely metabolized in the human body and will exist in the urine. The content of various substances in urine is usually used as an effective indicator for monitoring toxic substances in the human body and plays

 doi:10.20944/preprints202605.1703.v1

an important role in health assessment. Therefore, the development of reliable and sensitive methods to detect Lvx is a current health monitoring need.

Instrument methods for the detection of isoprocarb have high sensitivity, accuracy and repeatability, such as high performance liquid chromatography, gas chromatography, and spectrophotometry [3–5]. The reported methods such as high-performance liquid chromatography, enzyme-linked immunosorbent assay, electrochemical analysis, spectrophotometry, chemiluminescence, capillary electrophoresis and iodine determination have been applied to the detection of Lvx [6,7]. However, these above methods for the sensing of isoprocarb and Lvx have strict requirements for the pretreatment and handling of samples. The instrument method has some disadvantages such as long time, non-portability, expensive equipment, and complicated operation process, so it is difficult to meet the requirements for the monitoring of isoprocarb or Lvx in real-time field detection.

Metal compounds have wide application in the field of optics [8–16], electronics [17–19], magnetism, catalysis [20–31], gas adsorption and separation [32–35], bio-applications [36–43], and so on [44,45]. As one kind of metal compounds, lanthanide compounds have the unique fluorescence characteristics of large Stokes shift, long fluorescence lifetime, sharp emission band, etc. [46–54], and have great application potential in luminescent sensors [55–62]. Lanthanide complexes have the unique characteristics of rapid response, high sensitivity and real-time monitoring ability, which overcome the shortcomings of traditional methods and provide an effective technology and application prospect for molecular detection [63,64]. Based on the above shortcomings in detection efficiency, a dual fluorescence sensing system for isoprocarb and Lvx was established.

In summary, a new LnMOFs have been obtained and characterized in detail, and their fluorescence properties have been studied in detail. Interestingly, **EuMOFs** is a stable, fast, highly sensitive bifunctional sensor for isoprocarb and Lvx. Based on the study of fluorescence lifetime, UV-visible absorption and density functional theory (DFT), the sensing mechanisms were discussed. As an efficient pesticide responder, **EuMOFs** provides a new detection platform for isoprocarb residues in crops, and has great potential application value in food safety and human health. The developed fluorescence sensor can also detect Lvx in human urine effectively and quickly, which has extraordinary significance for human health and ecological environment.

2. Materials and Methods

2.1. Synthesis of EuMOFs

The ligand of 2,2-dihydroxyacetic acid ($C_2H_4O_4$, 8.51 mg, 0.092 mmol) and 1.0 mL H_2O were mixed evenly by ultrasonic treatment in a 10.0 mL flask for 5.0 min, and was adjusted to pH=5 with NaOH. 10.2 mg Eu $(NO_3)_3 \cdot 6H_2O$ (0.023 mmol) and 1.0 mL methanol were mixed in the second flask and sonicated for 5.0 min. The above two solutions were mixed evenly with ultrasonic treatment for 6.0 min, and then reacted for 3 days in 80 °C oven to obtain colorless massive crystals, high quality single-crystal were selected for single-crystal X-ray analysis.

$[Eu(OA)_{1.5} \cdot 3H_2O]_n$ (EuMOFs): Yield: 35.6%, based on Eu^{3+}. Anal. Calcd (%): C, 12.51, H, 2.10. Found (%): C, 13.05; H, 2.46. FT-IR (Figure S1) (KBr pellet, cm^{-1}): 3449(s), 2828(w), 2356(w), 2339(w), 2027(w), 1636(s),1586(w), 1387(m), 1351(m), 1269(w), 1082(s), 998(m), 769(m), 565(s), 468(w).

2.2. Preparation of Sensing Solution

Configuration of the **EuMOFs** solution: As synthesized **EuMOFs** was ground into a white powder and made into a transparent and homogeneous solution using DMF as the solvent (1.0×10^{-3} M, calculation by the molar of Eu^{3+}) for later use.

 doi:10.20944/preprints202605.1703.v1

Configuration of sensing solution: 50 μL **EuMOFs** stock solution (1.0×10^{-3} M) was dissolved in 4.9 mL of deionized water, and 50 μL of tested species water solution (1.0×10^{-3} M) mixed thoroughly before the fluorescence measurement. In the blank sample, 50 μL of tested species solution was replaced by 50 μL of deionized water. Real sample of tap water was collected from the water tap in our laboratory. Real sample of lake water was gathered from the Yao Lake near our university. The urine samples were provided by the researchers of this study, and the serum was purchased from Innochem. The real samples were filtered with 0.45 μm membrane filters prior to testing.

2.3. Computational Details

Quantum chemical studies were performed using density functional theory (DFT) implemented in GAUSSIAN 16 package [65,66]. Geometry optimization and single point energies are calculated at B3LYP functional with 6-31G(d) basis sets for other elements [67–71].

3. Results and Discussion

3.1. Crystal Structure Analysis

Single-crystal X-ray diffraction analyses reveal that **EuMOFs**, crystallizes in a triclinic space group *P*21/c and **EuMOFs** are in a Monoclinic space group *P*21/c. The crystallography data and structural refinement parameters of **EuMOFs** are listed in Table S1. **EuMOFs** crystalizes in the monoclinic *P*21/c space group, with a = 11.0633(7) Å, b = 9.5274(4) Å, c = 10.0760(8) Å, α = 90°, β = 114.423(8)°, γ = 90°, V = 967.02(12) Å^3, Z = 4. Each SBU contains one Eu^{3+}, one and half deprotonated oxalic acid that decomposition from 2,2-dihydroxyacetic acid, three coordination H_2O to form a neutral unit. The lanthanide ion is coordinated by 9 O to form polyhedral structure, where six O from the ligand of OA, and other three O are from coordinated H_2O (Figure 1a). The ligand of OA adopts a chelating coordination pattern (Figure S2). Two polyhedral structures are connected to form a dinuclear cluster structure (Figure 1b), the nine coordinated O around the metal center are arranged in a single truncated quadrangular prism structure (Figure S3). Three dinuclear clusters are connected in the *ac* plane to form a single-hole structure (Figure 1c), and the hole has a diameter of 8.93 Å. It further connects in the *oa* and *oc* directions through coordination bond to form a 2D porous MOFs structure (Figure 1d). The water contact angles of **EuMOFs** (Figure S4) sheet is in 77.6-78.8°, and lower than 90°, which is due to the fact that water easily forms hydrogen bonds with uncoordinated O. The coordination bond lengths are in normal range of 2.2981-2.588 Å for coordination compounds (Table S2) [72–74].

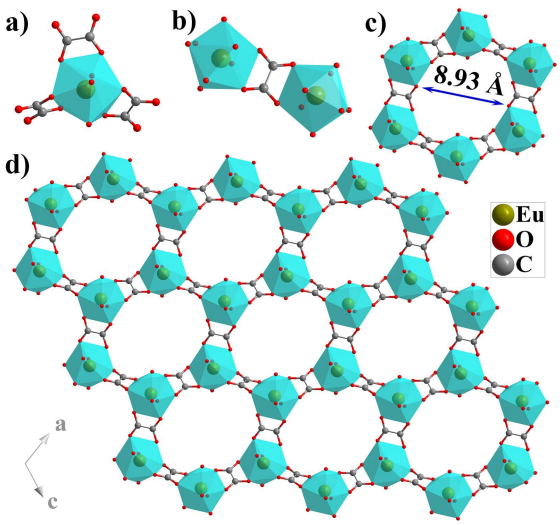

Figure 1. (a) SBU structure of **EuMOFs**; (b) the dinuclear cluster strucutre; (c) single hole structure constructed by three dinuclear cluster; (d) 2D porous MOFs structure of **EuMOFs**. .

 doi:10.20944/preprints202605.1703.v1

Powder X-ray Diffraction (PXRD). PXRD peaks of **EuMOFs** samples that soaked in pH = 2-12 solution, 9 kinds of organic solvents, water and exposed in the air for 2 h or longer time show that their diffraction peaks are consistent with the peaks of as-synthesized samples and their single crystal data (Figure 2), indicating highly stable characteristics of **EuMOFs**.

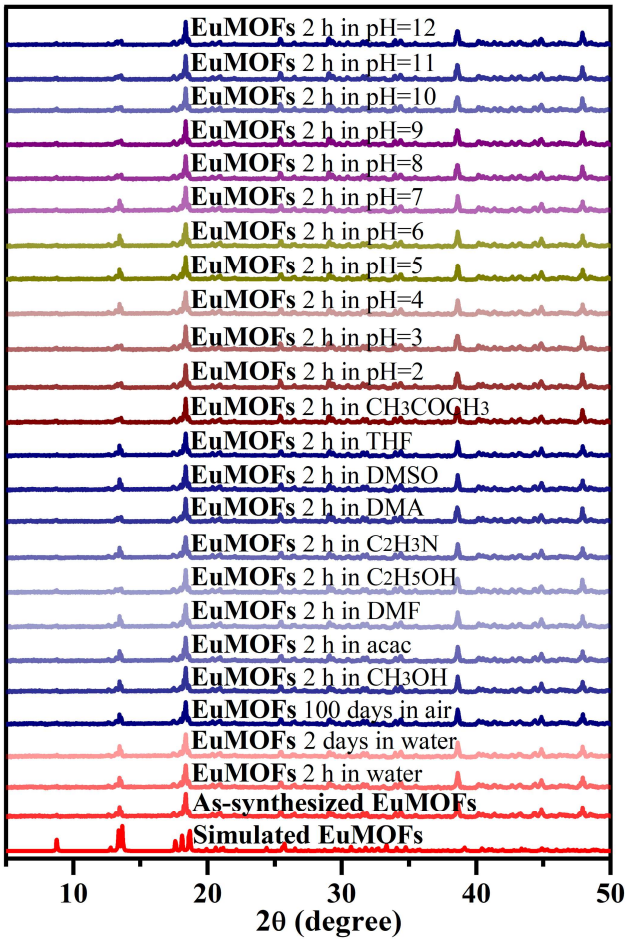

Figure 2. PXRD pattern of **EuMOFs** that immersed in pH = 2-12 solution, organic solvents, and soaked in water for 2 days and exposure in the atmosphere for 100 days.

3.2. Photophysical Studies

To study the photophysical properties of **EuMOFs**. The excitation and emission spectra, fluorescence lifetimes, and the fluorescence quantum yields of solid-state sample **EuMOFs** were measured at room temperature. As shown, wide excitation bands were observed in 210-350 nm, which were monitored at their maximum emission peak at 605 nm (Figure 3a). At the optimal excitation of 295 nm, **EuMOFs** emits four characteristic strong linear emission peaks in 550-750 nm, which are due to $^5D_0 \rightarrow {}^7F_1$, $^5D_0 \rightarrow {}^7F_2$, $^5D_0 \rightarrow {}^7F_3$, and $^5D_0 \rightarrow {}^7F_4$ transitions at 582, 605, 641, and 689 nm, respectively (Figure 3a) [75], which is a pure red fluorescence (CIE: 0.6255, 0.3740; Figure 3b). The photofluorescence quantum yield of **EuMOFs** is a relative high value of 9.81%. The maximum emission (605 nm) of the $^5D_0 \rightarrow {}^7F_2$ transition was selected to monitor its fluorescence lifetime, which fits a double exponential function (Figure 3c) and shows a long lifetime of 0.305 ms.

The fluorescence intensities of the electric-dipole transitions $^5D_0 \rightarrow {}^7F_2$ is greater than the $^5D_0 \rightarrow {}^7F_1$ magnetic dipole transitions, indicating that Eu^{3+} is in an irreversible symmetrical position, which are in line with its single crystal structure. Single crystals of **EuMOFs** were selected and photographed

 doi:10.20944/preprints202605.1703.v1

under natural light and 365 nm UV light, it was transparent (Figure S5a) and showed red fluorescence (Figure S5a′), respectively.

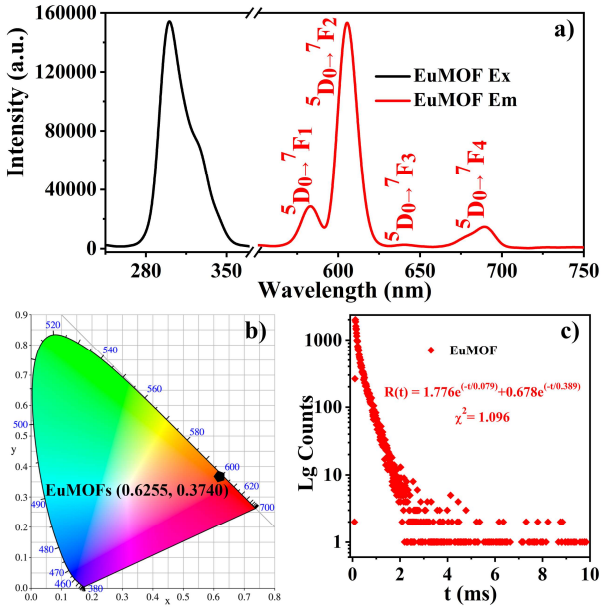

Figure 3. Solid-state photophysical studies for **EuMOFs** at room temperature: (a) excitation and emission spectra; (b) CIE coordinate graph; (c) fluorescence decays curve.

3.3. Sensing of Isoprocarb and Lvx

Isoprocarb is often residual in crops and foods, such as fruits and rice, which seriously endangers life and health. Lvx, a fluoroquinolone drug, is a broad-spectrum antibiotic, which is used more and more frequently, causing many diseases. Lvx has a strong ability to resist common biological decomposition, and the excessive use of Lvx is not completely metabolized in the human body and will exist in the urine. Therefore, there is an urgent need to explore ultra-sensitive and facile monitoring methods at the molecular level.

In the sensing, 15 kinds of cations of MCl_x or $M(NO_3)_y$, 11 kinds of anions of Na_mX, 24 kinds of organic solvents, 7 kinds of amino acids, 6 kinds of urea, 4 kinds of tumor markers, 4 kinds of floxacin drugs and 4 kinds of pesticides that listed in the supporting information (Section S1) were prepared into 1.0×10^{-3} M reserve solutions, respectively. 50 μL of the above 75 substances solution was mixed with 50 μL of 1.0×10^{-3} M **EuMOFs** reserve solution and 4.9 mL of deionized water, and then the mixed solution was placed at room temperature to react for 1.0 min. The luminescence histogram monitored at 605 nm ($^5D_0\rightarrow{}^7F_2$ transition) shows that among the 75 substances, only isoprocarb significantly quenched the fluorescence of Eu^{3+}, Lvx significantly enhanced the fluorescence of Eu^{3+} (Figure 4a), while other species did not change the fluorescence intensity of the solution markedly, suggesting **EuMOFs** is a highly selective sensor for isoprocarb and Lvx.

 doi:10.20944/preprints202605.1703.v1

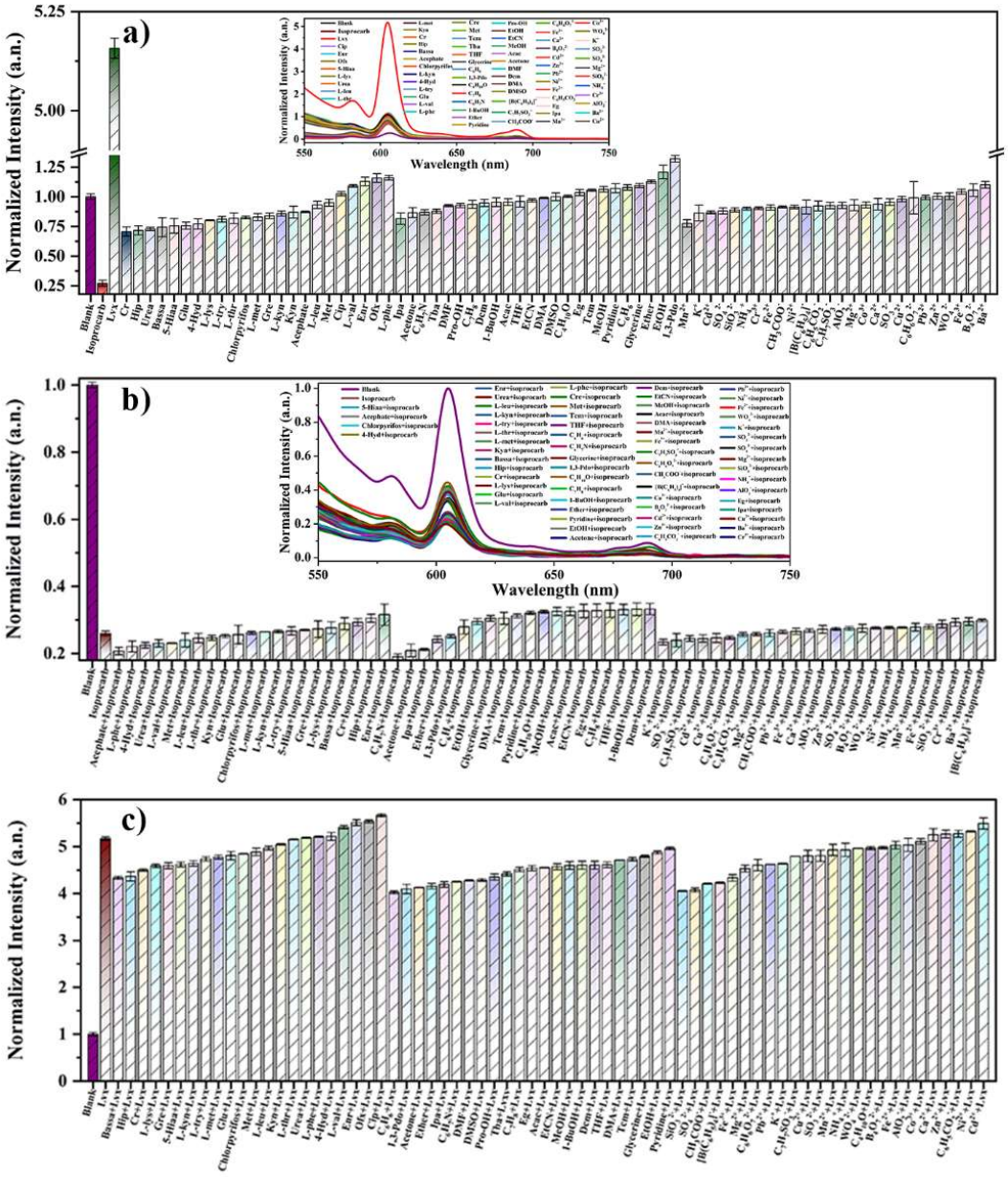

Figure 4. (a) Histogram of normalized fluorescence intensities at 605 nm of **EuMOFs** reacting with 75 substances, insert: full spectra; (b) histogram of fluorescence intensities of **EuMOFs** reacted to isoprocarb at the presence of 10 equiv. anti-interference species, insert: full spectra; (c) histogram of fluorescence intensities of **EuMOFs** reacted to Lvx at the presence of 10 equiv. anti-interference species. .

In real environments, the sensing results susceptible to be disturbed by other substances. To investigate whether the detection of isoprocarb and Lvx would be interfered by other substances, the competition experiment was performed. 4.4 mL deionized water was mixed with 50 μL **EuMOFs** stock solution (1.0×10^{-3} M), 50 μL isoprocarb or Lvx solution (1.0×10^{-3} M, H_2O) and 500 μL competitive substance (1.0×10^{-3} M H_2O). The fluorescence measurement of **EuMOFs** reacting with isoprocarb or Lvx in the presence of competing substances were determined by the above method. It shows that isoprocarb shows obvious fluorescence quenching at the presence of 10 equiv. anti-interference substances (Section S2, Figure 4b), Lvx shows obvious fluorescence enhancing in the presence of 10 equiv. anti-interference substances (Section S3, Figure 4c, Figure S6), revealing high anti-interference of the sensor.

 doi:10.20944/preprints202605.1703.v1

In addition, the reaction time of **EuMOFs** towards isoprocarb and Lvx were evaluated. The fluorescence intensity was monitored at 605 nm ($^5D_0 \rightarrow {}^7F_2$ transition), the dotted line shows that **EuMOFs** sensing isoprocarb (Figure 5a) and Lvx (Figure 5b) show fast response time of 15 s, and the sensing signal is stable within 1.0 hour, suggesting that **EuMOFs** is a highly stable sensor. In order to further understand the sensing characteristics of **EuMOFs**, the relationships between the fluorescence intensity of the sensor and the concentration of isoprocarb and Lvx were studied. It was found that the fluorescence intensity (605 nm) had excellent linear relationships with the concentration of isoprocarb and Lvx in 0.01-1.6 nM, which have linear equations of Y=-12565.83023X+46517.22573, R^2=0.99305 for isoprocarb (Figure 5c), and Y=19994.42895X+44839.92686, R^2=0.99162 for Lvx (Figure 5d). In a wide concentration range of 0.01-10.0 μM isoprocarb and Lvx concentration can be determined by fluorescence measurement as well, which satisfies the equation of Y=-3100.24992X+39164.71282, R^2=0.99561 for isoprocarb (Figure 5e), Y=24130.4125X+4192.16451, R^2=0.99807 for Lvx (Figure 5f). When 1.0×10^{-9} M isoprocarb reacts with 1.0×10^{-8} M **EuMOFs**, the ratio of signal to noise (S/N) is 5.17 (Figure 5g), revealing its LOD is as low as 1.0 nM, which is lower than the LOD value of the national standard (GB 28260-2011 for isoprocarb is 2.583 μM), indicating that **EuMOFs** is a highly sensitive probe for isoprocarb. When 5.0×10^{-10} M Lvx reacted with 1.0×10^{-9} M **EuMOFs**, the ratio of signal to noise (S/N) was 4.65, revealing its LOD is as low as 0.5 nM (Lvx, Figure 5h), which is lower than the LOD value of some other sensitive fluorescent probes (Table 1), indicating that **EuMOFs** is a highly sensitive probe for Lvx. The recovery rate of added samples in the sensing of isoprocarb and Lvx is between 97.86%-101.48% under various conditions in Table 2.

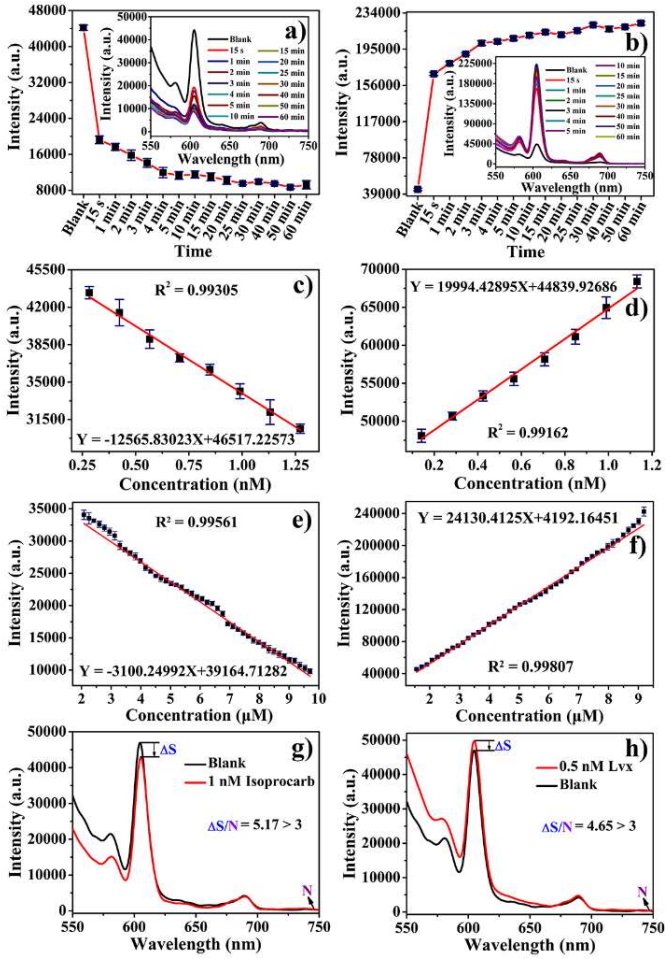

Figure 5. The dot plot of the fluorescence intensity at 605 nm of **EuMOFs** reacted with isoprocarb (a) and Lvx (b) at various reaction time, insert: full emission profiles; the linearity of fluorescence intensity versus the

 doi:10.20944/preprints202605.1703.v1

concentration of isoprocarb (c) and Lvx (d) that monitored at 605 nm; plot of fluorescence intensity (605 nm) of **EuMOFs** reacting with 0.01-10.0 μM isoprocarb (e) and Lvx (f); LOD measurement for sensing isoprocarb (g) and Lvx (h).

Table 1. LOD and linear range comparation of different methods for isoprocarb and Lvx detection.

Method	Analyte	Linear range (nM)	LOD (nM)	References
DPV	Isoprocarb	100-100000	79	[76]
Amperometry	Isoprocarb	100-150000	8	[3]
Chronoampermetry	Isoprocarb	5-1000	160	[4]
Luminescent detection	Isoprocarb	300-5200	260	[1]
UV-Vis detector	Isoprocarb	1000-50000	300	[5]
Differential Pulse Voltammetry	Lvx	5000-1000000	1800	[7]
Luminescent detection	Lvx	5000-150000	850	[2]
Luminescent detection	Lvx	53-110000	16	[77]
Luminescent detection	Lvx	2500-5000	1260	[6]
Luminescent detection	Lvx	100-400	20	[78]
EuMOFs	Isoprocarb	0-9000	1	**This work**
EuMOFs	Lvx	0-10000	0.5	**This work**

Table 2. Recovery results for the determination of isoprocarb and Lvx in water, apple peel supernatant, rice supernatant, and Urine by **EuMOFs**.

Sample	Analyte	Added (μM)	EuMOFs Recovery (%)	Theoretical value (μM)
Water	Isoprocarb	2.253	98.35	2.424
		3.813	99.85	3.826
		5.372	100.32	5.349
		6.932	98.38	7.024
		8.492	99.45	8.515
Apple peel supernatant	Isoprocarb	2.253	100.12	2.239
		3.813	99.58	3.852
		5.372	99.28	5.428
		6.932	100.37	6.909
		8.492	99.39	8.520
Rice supernatant	Isoprocarb	2.253	100.87	2.174
		3.813	99.12	3.879
		5.372	100.78	5.325
		6.932	99.89	6.937
		8.492	100.57	8.476
Urine	Isoprocarb	2.079	99.16	2.060
		3.640	101.48	3.696

 doi:10.20944/preprints202605.1703.v1

Water	Lvx	5.199	98.65	5.126
		6.759	100.38	6.785
		8.318	97.86	8.136
		2.079	99.61	2.067
		3.640	101.25	3.698
Urine	Lvx	5.199	99.92	5.194
		6.759	100.66	6.810
		8.318	99.57	8.278

In addition, whether **EuMOFs** can be used as a luminescent probe for the detection of isoprocarb in actual sample of apple peel (Section S4) and rice supernatant (Section S5), and for the probe of Lvx in urine (Section S6) were further investigated. 4.9 mL apple peel or rice supernatant mixed with 50 μL **EuMOFs** solution (1.0×10^{-3} M, DMF) and 50 μL 1.0×10^{-3} M isoprocarb, respectively. 4.9 mL urine solution mixed with 50 μL stock **EuMOFs** solution (1.0×10^{-3} M, DMF) and 50 μL 1.0×10^{-3} M Lvx, respectively. It shows that **EuMOFs** reacted with isoprocarb in apple peel supernatant, rice supernatant showed obvious fluorescence quenching for isoprocarb, and Lvx in urine showed obvious fluorescence quenching, confirming that **EuMOFs** has great potential application in the detection of isoprocarb in real samples of apple peel supernatant, rice supernatant, and Lvx in real urine (Figure 6).

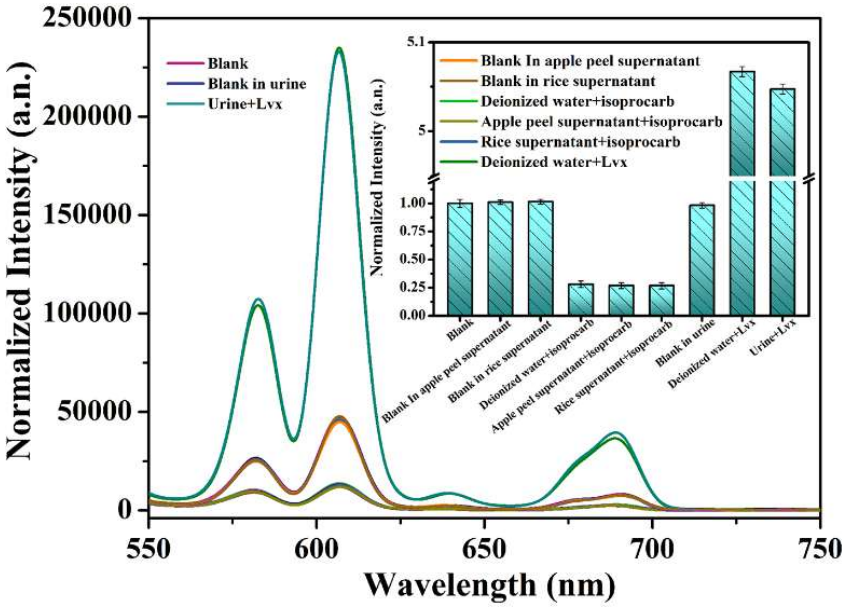

Figure 6. Full spectrum of fluorescence of **EuMOFs** reacted with isoprocarb and Lvx in real samples of apple peel supernatant, rice supernatant, and in urine, insert: fluorescence histogram.

It is found that the fluorescence intensity (605 nm) has excellent linear relationships with isoprocarb concentration in 0.01-1.6 nM in the real samples of apple peel supernatant, rice supernatant, and has excellent linear relationships with Lvx concentration in urine, which have linear equations of Y =-13697.23628X+46976.39555, R^2=0.9925 for isoprocarb in apple peel supernatant (Figure 7a), Y=-12652.30395X+46769.17802, R^2=0.9951 for isoprocarb in rice supernatant (Figure 7b), and Y=18104.3278X+39563.96478, R^2=0.99436 for Lvx in urine (Figure 7c). In a wide concentration range of 0.01-9.0 μM in apple peel and rice preparation solution, isoprocarb concentration can be determined by fluorescence measurement as well, which satisfies the equation of Y=-3436.03363X+45003.13694, R^2=0.99503 in apple peel supernatant (Figure 7d) and Y=-

 doi:10.20944/preprints202605.1703.v1

4364.02963*X*+49589.00671, R^2=0.9941 in rice supernatant (Figure 7e). In the concentration range of 0.01-9.0 μM in urine, Lvx concentration can be determined by fluorescence measurement as well, which satisfies the equation of *Y*=23275.10227*X*+23158.99165, R^2=0.99457 (Figure 7f). When 1.0×10^{-9} M isoprocarb reacted with 1.0×10^{-8} M **EuMOFs** in apple peel and rice supernatant respectively, the ratio of signal to noise (S/N) is 4.82 and 5.32, respectively, revealing its LOD is as low as 1.0 nM (Figure 7g, 7h), which is lower than the LOD value of the national standard (GB 28260-2011, isoprocarb 2.583 μM), indicating that **EuMOFs** is a highly sensitive probe for isoprocarb in apple peel and rice supernatant. And when 5.0×10^{-10} M Lvx reacts with 1.0×10^{-9} M **EuMOFs** in urine, the ratio of signal to noise (S/N) is 4.35, suggesting its LOD is as low as 0.5 nM (Figure 7i), which is lower than the LOD value of other fluorescent probes in Table 2, indicating **EuMOFs** is a highly sensitive probe for Lvx in real sample. The recovery rates of isoprocarb and Lvx the above in real samples were between 99.12%-101.25% (Table 3), further confirmed the reliability and practicability of the sensing method of this work.

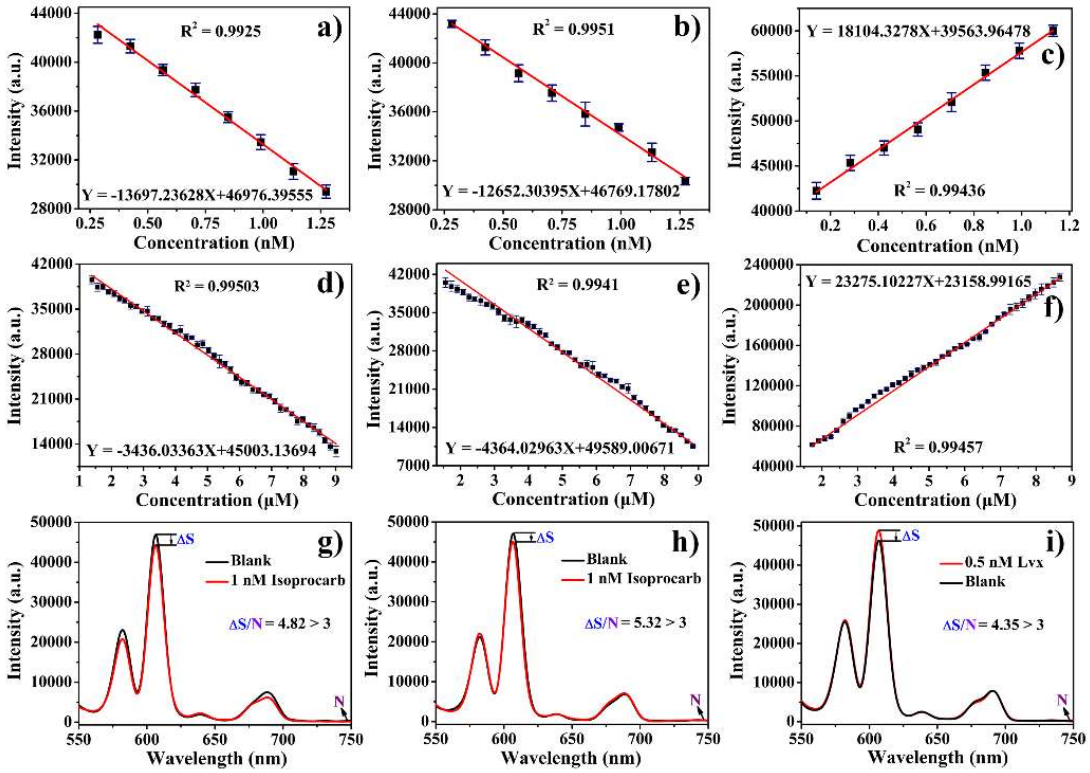

Figure 7. Plot of fluorescence intensity (605 nm) of **EuMOFs** reacting with isoprocarb in real samples of apple peel supernatant (a), rice supernatant (b) and with Lvx in real samples of urine (c); the linearity of fluorescence intensity versus the concentration of 0.01-9.0 μM isoprocarb in apple peel supernatant (d), in rice supernatant (e) and 0.01-9.0 μM Lvx in urine (f) at 605 nm; LOD measurement for sensing isoprocarb in real samples of apple peel supernatant (g), rice supernatant (h) and Lvx in real samples of urine (i).

The results of sensing is superior than that reported methods listed in Table 1. Compared with other detection methods, the sensor developed in this work has the advantages of simple preparation, low LOD value, high sensitivity and wide linear range.

 doi:10.20944/preprints202605.1703.v1

Table 3. Recovery results for the determination of isoprocarb and Lvx in water, apple peel supernatant, rice supernatant, and Urine by **EuMOFs**.

Sample	Analyte	Added (μM)	EuMOFs Recovery (%)	Theoretical value (μM)
Water	Isoprocarb	2.253	98.35	2.424
		3.813	99.85	3.826
		5.372	100.32	5.349
		6.932	98.38	7.024
		8.492	99.45	8.515
Apple peel supernatant	Isoprocarb	2.253	100.12	2.239
		3.813	99.58	3.852
		5.372	99.28	5.428
		6.932	100.37	6.909
		8.492	99.39	8.520
Rice supernatant	Isoprocarb	2.253	100.87	2.174
		3.813	99.12	3.879
		5.372	100.78	5.325
		6.932	99.89	6.937
		8.492	100.57	8.476
Water	Lvx	2.079	99.16	2.060
		3.640	101.48	3.696
		5.199	98.65	5.126
		6.759	100.38	6.785
		8.318	97.86	8.136
Urine	Lvx	2.079	99.61	2.067
		3.640	101.25	3.698
		5.199	99.92	5.194
		6.759	100.66	6.810
		8.318	99.57	8.278

3.4. Sensing Mechanism

EuMOFs that reacted with 1.0×10^{-5} M isoprocarb and Lvx were washed by 3×5.0 mL water and measured by PXRD. The results confirmed the samples were in line with as-synthesized **EuMOFs**, and no peaks in line with isoprocarb or Lvx appeared, confirming the structure of **EuMOFs** remain integrity after sensing (Figure S7). The fluorescence lifetimes of **EuMOFs** blank solution (1.0×10^{-5} M) and **EuMOFs** solution (1.0×10^{-5} M) reacted with isoprocarb (1.0×10^{-5} M) or Lvx (1.0×10^{-5} M) are 0.281, 0.242, and 1.862 ms (Figure 8a), the photoluminescence quantum yields are 7.52%, 6.86% and 13.54%, respectively, revealing the lifetimes of the sensing samples for isoprocarb are shorter than blank solution and for Lvx are longer than blank solution, and their fluorescence quantum yield are in line with their lifetimes, revealing the sensing of isoprocarb is a dynamic quenching process and Lvx is a dynamic enhancing process.

The LUMO level of Lvx (-2.2476) is smaller than the LUMO level of isoprocarb (-0.9306) (Figure 8b), and the LUMO level of Lvx is closer to the energy level of Eu^{3+}, which is easier to transfer energy

 doi:10.20944/preprints202605.1703.v1

to Eu^{3+}, so the fluorescence is enhanced. The LUMO energy level of isoprocarb to Eu^{3+} is more suitable to Eu^{3+} than Lvx, so the fluorescence of sensing isoprocarb is decreased [79].

Table 4. HOMO and LUMO Energies for the isoprocarb, Lvx and Eu^{3+}.

Analytes	HOMO (eV)	LUMO (eV)	Band gap (ev)
Isoprocarb	-0.9306	-3.4021	2.4715
Lvx	-2.2476	-4.8541	2.6065

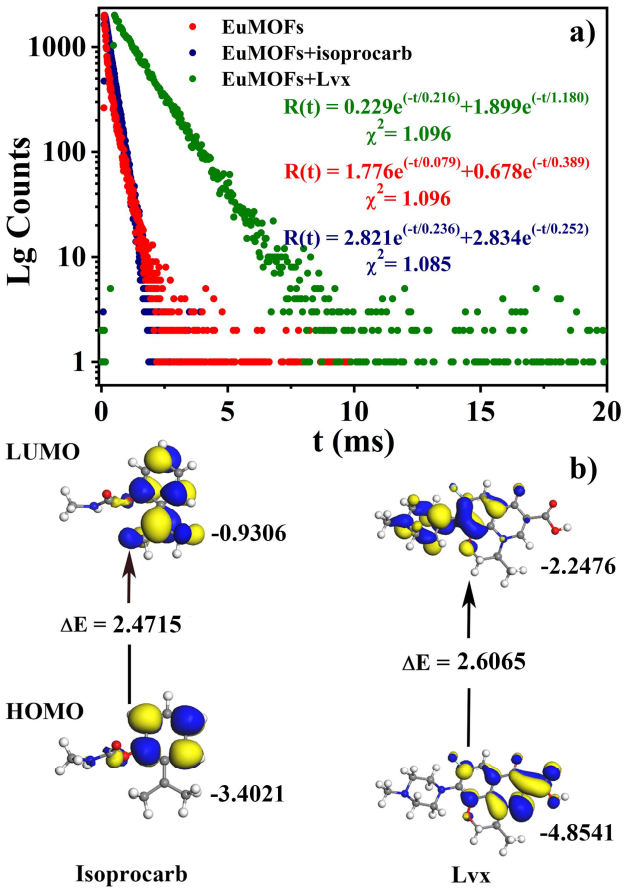

Figure 8. (a) Fluorescence lifetime decay curves of samples **EuMOFs**, **EuMOFs**+isoprocarb and **EuMOFs**+Lvx; (b) HOMO and LUMO of isoprocarb and Lvx.

4. Conclusions

In summary, a porous lanthanide MOFs of **EuMOFs** has been obtained and their fluorescence properties have been studied in detail. Interestingly, **EuMOFs** was a bi-functional sensor for isoprocarb and Lvx, which showed excellent anti-interference ability, rapid response of 15 s, excellent linear relationship and wide linear range, LODs as low as 1.0 nM and 0.5 nM, respectively. In addition, **EuMOFs** has also been successfully applied to the detection of isoprocarb in apple peel and rice supernatant, and sensing of Lvx in real urine, which still has high selectivity for isoprocarb and Lvx in actual samples, excellent anti-interference ability, and excellent detection stability in the linear range of 0.01~9.0 nM. The recoveries for the two species sensing were in 99.12%~101.25%. The LOD for isoprocarb detection in apple peel and rice supernatant was as low as 1.0 nM, and for Lvx detection in urine was as low as 0.5 nM, with excellent reproducibility and recovery. The sensor has

 doi:10.20944/preprints202605.1703.v1

a higher sensitivity for isoprocarb and Lvx than previously reported fluorescence sensors or maximum residue limit levels (GB 28260-2011, isoprocarb 2.583 μM). More interestingly, it allows specific detection of isoprocarb residues in crop food samples and Lvx in human urine. Based on the investigation of fluorescence lifetime and DFT, the sensing mechanisms were investigated. As an efficient pesticide response substance, **EuMOFs** provides a new detection platform for isoprocarb residues in crops, and has great potential application value in food safety and human health. The highly sensitive and quickly detection of Lvx in human urine shows extraordinary significance for human health.

Supplementary Materials: The following supporting information can be downloaded at the website of this paper posted on Preprints.org.

Author Contributions: The work presented here was carried out as a collaboration among all authors. Conceptualization, methodology, and formal analysis, Y.Y., C.H., and C.Z.; writing—original draft preparation, Y.Y., N.S., and C.H.; writing—review and editing, N.S. and C.Z.; funding acquisition, C.Z. All authors have read and agreed to the published version of the manuscript.

Institutional Review Board Statement: Not applicable.

Informed Consent Statement: Not applicable.

Data Availability Statement: The data will be made available upon request.

Funding: This research was funded by Jiangxi Provincial Natural Science Foundation (20232ACB213006).

Conflicts of Interest: The authors declare no conflicts of interest.

References

1. Zhu, Y. A.; Wang, M.; Zhang, X. G.; Cao, J.; She, Y. X.; Cao, Z.; Wang, J.; Abd El-Aty, A. M. Acetylcholinesterase Immobilized on Magnetic Mesoporous Silica Nanoparticles Coupled with Fluorescence Analysis for Rapid Detection of Carbamate Pesticides. *Acs Appl. Nano Mater.* **2022**, *5*, 1327-1338.
2. Shi, Y. Q.; Wu, Q. C.; Li, W. T.; Lin, L.; Qu, F. F.; Shen, C. J.; Wei, Y. Z.; Nie, P. C.; He, Y.; Feng, X. P. Ultra-sensitive detection of hydrogen peroxide and levofloxacin using a dual-functional fluorescent probe. *J. Hazard. Mater.* **2022**, *432*, 128605.
3. Jiao, W.; Ding, G. Y.; Wang, L.; Liu, Y.; Zhan, T. R. Polyaniline functionalized CoAl-layered double hydroxide nanosheets as a platform for the electrochemical detection of carbaryl and isoprocarb. *Microchim. Acta* **2022**, *189*, 78.
4. Rachmawati, A.; Sanjaya, A. R.; Putri, Y.; Gunlazuardi, J.; Ivandini, T. A. An acetylcholinesterase-based biosensor for isoprocarb using a gold nanoparticles-polyaniline modified graphite pencil electrode. *Anal. Sci.* **2023**, *39*, 911-923.
5. Hsu, C. H.; Hu, C. C.; Chiu, T. C. Analysis of carbofuran, carbosulfan, isoprocarb, 3-hydroxycarbofuran, and 3-ketocarbofuran by micellar electrokinetic chromatography. *J. Sep. Sci.* **2012**, *35*, 1359-1364.
6. Liang, X.; Liu, H. M.; Du, Y.; Li, W. Z.; Wang, M.; Ge, B.; Zhao, L. M. Terbium functionalized covalent organic framework for selective and sensitive detection of LVX based on fluorescence enhancement. *Colloid. Surface. A* **2020**, *606*, 125429.
7. Zhad, H.; Lai, R. Y. Iron(III)-mediated Electrochemical Detection of Levofloxacin in Complex Biological Samples. *Electroanalysis* **2017**, *29*, 2672-2677.
8. Cai, S. T.; Huang, Z. L.; Liu, C.; Liu, Q. C.; Cao, S. H.; Zeng, X. S. A NIR-emitting fluorescent probe based on se-substituted xanthene-cyanine for bioimaging endogenous H_2O_2 in autophagy and tumors. *Spectrochim. Acta A* **2026**, *348*, 127184.
9. Zhang, N. N.; Wang, H. Y.; Yan, X. Y.; Wang, X. P.; Liu, B.; Zhang, Y. Y.; Yang, Y. G. Deep-red emitting $La_3Ga_5SiO_{14}:Mn^{4+}$phosphors with outstanding thermal stability. *J. Mol. Struct.* **2025**, *1325*, 141066.
10. Xia, Y. P.; Huang, Y. X.; Li, H. H.; Li, X. T.; Zheng, Z. P.; Zhou, F. Mechanochemical-assisted synthesis of a novel sandwich-structured coronene/trinuclear silver(I) pyrazolate donor-acceptor cocrystal: structure, spectroscopic, Hirshfeld surfaces and DFT studies. *J. Mol. Struct.* **2025**, *1340*, 142579.

 doi:10.20944/preprints202605.1703.v1

11. Liu, L. R.; Liu, S. Y.; Han, D. D.; Meng, Q. G.; Niu, C.; Wang, Z. Q.; Xin, X. L. A Multifunctional Cyclodextrin-based Metal-organic Material for the Visual and Selective Detection of Ag^{+} and Adsorption of Congo Red. *Curr. Anal. Chem.* **2025**, *22*, 851-860.
12. Zhou, X. J.; Liu, L. L.; Wu, D. X.; Niu, Y.; Zheng, S. M.; Lu, J. T.; Feng, Y. M.; Tai, X. S. A Luminescent Cd-MOF Used as a Chemosensor for High-Efficiency Sensing of Fe^{3+}, Cr(IV), Trinitrophenol, and Colchicine. *Acs Omega* **2024**, *9*, 11339-11346.
13. Wang, J.; Song, M. J.; Xue, J. P.; Bi, S. L.; Seo, H. J. Luminescence properties of Bi^{3+}/Sm^{3+} co-doped $K_3Gd_5(PO_4)_6$ phosphors for self-referencing optical thermometry. *Rsc Adv.* **2024**, *14*, 31398-31408.
14. Zeng, W.; Wang, X.; Kong, X.; Li, Y.; Zhang, Y. Study on crystal structure, spectroscopic, thermodynamic properties and Hirshfeld surfaces of a new spirocompound containing thiourea group $C_{17}H_{18}N_2O_4S$. *J. Mol. Struct.* **2023**, *1279*, 135017.
15. Abdurahman, A.; Wang, J.; Zhao, Y.; Li, P.; Shen, L.; Peng, Q. A Highly Stable Organic Luminescent Diradical. *Angew. Chem. Int. Ed.* **2023**, *62*, e202300772.
16. Zhou, W. W.; Xv, L.; Zheng, Q. H.; Wang, F. W.; Liu, F. F.; Yue, L.; Qian, Y. W.; Song, M. J.; Xie, Z.; Zhao, W. Sandwich heterometallic coordination polymers consisting of copper-cluster pillars and layered networks of $\{Ln_6\}$ wheels: synthesis, structures, spectroscopic properties and Judd-Ofelt analysis. *Transition Met. Chem.* **2021**, *46*, 555-564.
17. Yu, M. Y.; Li, X. Z.; Zhang, L.; Jia, Y. L.; Zou, F.; Liu, Z. L.; Zhang, X. W.; Zhang, Q.; Liu, J. H.; Li, W.; Wang, Y. Q. Recent Advances in Polyoxometalate-Based Materials as Anodes for Lithium-Ion Batteries. *Chemistryselect* **2025**, *10*, e03244.
18. Niu, X. K.; Zheng, N.; Liao, M. L.; Zhu, Q. Q.; Tian, H. Y.; Lu, J. T.; Zhang, X. M. $Cu_{x+1}O$-mediated photo-nanozyme-integrated photoelectrochemical-colorimetric dual-readout biosensing for sensitive detection of MiRNA. *Sens. Actuators B Chem.* **2025**, *444*, 138383.
19. Liu, J. H.; Liu, D.; Yu, M. Y.; Liu, L.; Wang, Y. Q.; Huo, Y. F.; Sun, S. Q.; Hao, S. S. Manganese-Resorcin 4 Arene-Based Metal-Organic Framework: Syntheses, Structure and Lithium-Ion Battery Application. *Eur. J. Inorg. Chem.* **2025**, *28*, e202400785.
20. Xi-Shi, T.; Li-Hua, W.; Al-Resayes, S. I.; Azam, M. A new 3D Ba(II) coordination polymer based on 3-(3-carboxyphenyl)-isonicotinic acid: structural studies and its catalytic role in benzylic alcohol oxidation. *Polyhedron* **2026**, *289*, 118009.
21. Tai, X. S.; Wang, L. H.; Al-Resayes, S. I.; Azam, M. Synthesis, structural characterization, Hirschfeld surface analysis and catalytic application of a new cd(II) complex bearing 1H-pyrazolo 3,4-b pyridine-3-amine and pyridine carboxylic acid. *Polyhedron* **2025**, *279*, 117647.
22. Lu, H.; Fu, D.; Tai, X. S.; Sun, Z. L.; Wang, X. K. Metal-Organic Frameworks/Covalent-Organic Frameworks-Based Materials in Organic/inorganic Pollutant Elimination and CO_2 Reduction Applications. *Chemnanomat* **2025**, *11*, e202500244.
23. Liu, L. L.; Zang, M. L.; Li, L.; Zhang, Y. K.; Wang, L. Y.; Zhou, X. J.; Xin, C. L.; Tai, X. S. MIL-53(Al)-derived bimetallic Pd-Co catalysts for the selective hydrogenation of 1,3-butadiene at low temperature. *Sci. Rep.* **2025**, *15*, 448.
24. Tai, X. S.; Yan, X. H.; Wang, L. H. Synthesis, Structural Characterization, Hirschfeld Surface Analysis, Density Functional Theory, and Photocatalytic CO_2 Reduction Activity of a New Ca(II) Complex with a Bis-Schiff Base Ligand. *Molecules* **2024**, *29*, 1047.
25. Liu, Y.; Tang, X.; Yan, X. H.; Wang, L. H.; Tai, X. S.; Azam, M.; Zhao, D. Q. The Synthesis, Structural Characterization, and DFT Calculation of a New Binuclear Gd(III) Complex with 4-Aacetylphenoxyacetic Acid and 1,10-Phenanthroline Ligands and Its Roles in Catalytic Activity. *Molecules* **2024**, *29*, 3039.
26. Cui, Y.; Chen, Y. S.; Cao, Z.; Xu, L. L.; He, J.; Zhu, Z. H.; Lian, L. S.; Luo, X.; Yang, Z. Y.; Chen, M. D. Oxidation of Toluene over the Pt-Embedded Mesoporous CeO_2 Hollow Nanospheres with Advanced Catalytic Performances. *Inorg. Chem.* **2024**, *63*, 19972-19990.
27. Wang, L. H.; Tai, X. S. Synthesis, Structural Characterization, Hirschfeld Surface Analysis and Photocatalytic CO_2 Reduction Activity of a New Dinuclear Gd(III) Complex with 6-Phenylpyridine-2-Carboxylic Acid and 1,10-Phenanthroline Ligands. *Molecules* **2023**, *28*, 7595.

 doi:10.20944/preprints202605.1703.v1

28. Wu, Q.; Gao, Q. P.; Sun, L. M.; Guo, H. M.; Tai, X. S.; Li, D.; Liu, L.; Ling, C. Y.; Sun, X. P. Facilitating active species by decorating CeO_2 on Ni_3S_2 nanosheets for efficient water oxidation electrocatalysis. *Chin. J. Catal.* **2021**, *42*, 482-489.
29. Lu, J.; Zhang, H.; Li, S.; Guo, S.; Shen, L.; Zhou, T.; Zhong, H.; Wu, L.; Meng, Q.; Zhang, Y. Oxygen-Vacancy-Enhanced Peroxidase-like Activity of Reduced Co_3O_4 Nanocomposites for the Colorimetric Detection of H_2O_2 and Glucose. *Inorg. Chem.* **2020**, *59*, 3152-3159.
30. Lu, J. T.; Zeng, Y.; Ma, X. X.; Wang, H. Q.; Gao, L. N.; Zhong, H.; Meng, Q. G. Cobalt Nanoparticles Embedded into N-Doped Carbon from Metal Organic Frameworks as Highly Active Electrocatalyst for Oxygen Evolution Reaction. *Polymers* **2019**, *11*, 828.
31. Zhang, S.; Lu, L.; Jiang, J.; Liu, N.; Zhao, B.; Xu, M.; Cheng, P.; Shi, W. Organizing Photosensitive and Photothermal Single-Sites Uniformly in a Trimetallic Metal-Organic Framework for Efficient Photocatalytic Hydrogen Evolution. *Adv. Mater.* **2024**, *36*, 2403464.
32. Zhao, X. Y.; Chang, X. T.; Qin, C. X.; Wang, X. K.; Xu, M. M.; Fan, W. D.; Meng, Q. G.; Sun, D. F. Solvent Regulation in Layered Zn-MOFs for C_2H_2/CO_2 and CO_2/CH_4 Separation. *Molecules* **2025**, *30*, 1171.
33. Xu, M. M.; Li, Y.; Wang, X. K.; Liu, H. Y.; Liu, Q. R.; Zhang, Y. F.; Fan, W. D.; Meng, Q. G.; Sun, D. F. Imidazole-Functionalized Zn-MOFs for One-Step C_2H_4 Purification from $C_2H_2/C_2H_4/C_2H_6$ Ternary Mixture. *Inorg. Chem.* **2025**, *64*, 813-817.
34. Gao, X.; Yan, W. H.; Hu, B. Y.; Huang, Y. X.; Zheng, S. M. Porous Metal-Organic Frameworks for Light Hydrocarbon Separation. *Molecules* **2023**, *28*, 6337.
35. Xin, C. L.; Ren, Y.; Zhang, Z. F.; Liu, L. L.; Wang, X.; Yang, J. M. Enhancement of Hydrothermal Stability and CO_2 Adsorption of Mg-MOF-74/MCF Composites. *Acs Omega* **2021**, *6*, 7739-7745.
36. Wang, L. H.; Tai, X. S.; Azam, M.; Sui, B. L.; Wang, A. L. Synthesis, structural characterization, and Hirschfeld surface analysis of a novel Mn(II) complex based on N-acetyl-L-phenylalanine ligand and its evaluation as a cytotoxic agent. *Polyhedron* **2025**, *279*, 117659.
37. Chen, W.; Sun, J. R.; Xiao, H. Y.; Zhu, Z. F.; Xing, J. Q.; Zhang, Y. B.; Shen, L.; Wang, Y. F. Near-infrared hemicyanine photosensitizer for targeted mitochondrial viscosity imaging and efficient photodynamic therapy. *Spectrochim. Acta A* **2025**, *325*, 125049.
38. Cao, S. H.; Tai, X. S.; Li, K. X.; Zhang, A. L.; Ma, P. J.; Sui, G. Q.; Zhang, L. S.; Tian, X. H.; Wang, A. L.; Azam, M. Two novel homo/hetero polynuclear complexes for DNA binding, molecular docking and anti-cancer activity. *J. Mol. Struct.* **2025**, *1325*, 141040.
39. Cao, S. H.; Liu, Y. C.; Tai, X. S.; Shen, L.; Yang, H. K.; Li, F. H.; Sui, B. L.; Ma, P. J.; Zhu, L. X.; Gao, B.; Wang, A. L.; Azam, M. A dual-type I/II NIR photosensitizer for effective cancer photodynamic therapy with enhanced ROS generation. *Rsc Adv.* **2025**, *15*, 28889-28896.
40. Yang, Y. D.; Niu, X. K.; Duan, B. Q.; Lu, J. T.; Zhang, X. M. Dual-modal biosensor for mercuric ion detection based on Cu_2O@Cu_2S/D-TA COF heterojunction with excellent catalase-like, electrochemical and photoelectrochemical properties. *Biosens. Bioelectron.* **2024**, *262*, 116568.
41. Cao, S. H.; Wang, A. L.; Li, K. X.; Lin, Z. T.; Yang, H. W.; Zhang, X. L.; Qiu, J. M.; Tai, X. S. A novel tetranuclear Cu(ii) complex for DNA-binding and in vitro anticancer activity. *Rsc Adv.* **2023**, *13*, 26324-26329.
42. Cao, S. H.; Tai, X. S.; Xin, C. L. Synthesis, Crystal Structure and Antitumor Activity of a Ca(II) Coordination Polymer Based on 4-Acetylphenoxyacetate Ligands. *Chin. J. Struct. Chem.* **2021**, *40*, 324-328.
43. Tai, X. S.; Zhou, X. J.; Liu, L. L. Synthesis, Crystal Structure and Antitumor Activity of a Na(I) Coordination Polymer Based on 2-Propyl-4,5-imidazoledicarboxylic Acid and 1,10-Phenanthroline Ligands. *Chin. J. Struct. Chem.* **2019**, *38*, 1079-1085.
44. Xie, N. B.; Wang, M.; Ji, T. T.; Guo, X.; Gang, F. Y.; Hao, Y.; Zeng, L.; Wang, Y. F.; Feng, Y. Q.; Yuan, B. F. Simultaneous detection of 5-methylcytosine and 5-hydroxymethylcytosine at specific genomic loci by engineered deaminase-assisted sequencing. *Chem. Sci.* **2024**, *15*, 10073-10083.
45. Cai, D. G.; Pan, S. F.; Zheng, T. F.; Cao, C.; Hu, Z. B.; Peng, Y.; Wu, Y. Q.; Wen, H. R.; Liu, S. J. pH- and Solvent-Stable ZnII/CdII Metal-Organic Frameworks with 2,1,3-Benzothiadiazole Derivative for Turn-On Fluorescence Sensing Dipicolinic Acid and Thiamine in Living Cells. *Anal. Chem.* **2026**, *98*, 5205-5213.

 doi:10.20944/preprints202605.1703.v1

46. Li, H. H.; Wu, Y.; Shoaib, M.; Sheng, W.; Bei, Q. Y.; Murugesan, A. Lanthanide-Doped Upconversion Luminescence: A New Frontier in Pathogenic Bacteria and Metabolite Detection from Design to Point-of-Care Application. *Chemosensors* **2025**, *13*, 60.
47. Xia, Z. R.; Li, R. Q.; Liu, F. F.; Zhou, W. W.; Zhao, W.; Meng, W.; Song, M. J.; Xue, J. P. Dual-luminescent $Sc_2(MoO_4)_3$:Dy^{3+}/Eu^{3+} phosphor system: energy transfer dynamics and high-sensitivity temperature sensing. *Rsc Adv.* **2025**, *15*, 28994-29002.
48. Song, M. J.; Zhou, W. W.; Wang, J.; Wang, M. Q.; Zhao, J. Q.; Ran, W. G. Multicolor luminescence and high efficient optical thermometric performance of Eu^{3+} and Sm^{3+} in self-activated $Na_2LuMg_2V_3O_{12}$ garnet. *J. Rare Earth* **2025**, *43*, 2357-2367.
49. Song, M.; Wang, J.; Xie, Z.; Liu, L.; Zhao, W.; Zhou, W. Spectroscopic and temperature sensing properties of Sm^{3+} in self-activated $CsLu(WO_4)_2$ phosphors. *J. Rare Earth* **2024**, *42*, 2033-2042.
50. Cao, E. S.; Zhang, Y. X.; Sun, L.; Sun, B.; Hao, W. T.; Zhang, Y. J.; Nie, Z. Q. WO_3-$LaFeO_3$ Nanocomposites for Highly Sensitive Detection of Acetone Vapor at Low Operating Temperatures. *Chemosensors* **2023**, *11*, 439.
51. Wang, M.; Han, Z.; Wang, K.; Zhao, B.; Sun, T.; Wu, Y.; Cheng, P.; Shi, W. Confinement of P-Xylene in the Pores of a Bilanthanide Metal-Organic Framework for Highly Selective Recognition. *Angew. Chem. Int. Ed.* **2024**, *63*, e202318722.
52. Wang, H.-L.; Li, Y.-L.; Zou, H.-H.; Liang, F.-P.; Zhu, Z.-H. Smart Lanthanide Metal-Organic Frameworks with Multicolor Luminescence Switching Induced by the Dynamic Adaptive Antenna Effect of Molecular Rotors. *Adv. Mater.* **2025**, *37*, 2502742.
53. Li, Y.-L.; Wang, H.-L.; Zhu, Z.-H.; Liang, F.-P.; Zou, H.-H. Recent advances in the structural design and regulation of lanthanide clusters: Formation and self-assembly mechanisms. *Coord. Chem. Rev.* **2023**, *493*, 215322.
54. Zhao, D.; Guo, L.; Li, Q.; Yue, C.; Han, B.; Liu, K.; Li, H. Multi-Functional Lanthanide Metallopolymer: Self-Healing and Photo-Stimuli-Responsive Dual-Emitting Luminescence for Diverse Applications. *Adv. Mater.* **2024**, *36*, 2405164.
55. Ahmed, D.; Spagnoli, E.; Chakir, A.; Mancinelli, M.; Ferroni, M.; Mehdaoui, B.; El Bouari, A.; Fabbri, B. $PrFeTiO_5$-Based Chemoresistive Gas Sensors for VOCs Detection. *Chemosensors* **2025**, *13*, 222.
56. Lopes, G. P.; Rossato, J. H. H.; Carreno, N. L. V.; Nantes, I. L.; Escote, M. T. Eu-Doped Nickelate as a Platform for an Enzyme-Based Resistive Biosensor for Glucose. *Chemosensors* **2025**, *13*, 387.
57. Yu, Q. B.; Wang, M.; Feng, X. J.; Li, X. H. Research Progress of Rare Earth Metal-Organic Frameworks on Pollutant Monitoring. *Chemosensors* **2025**, *13*, 184.
58. Zhou, X.; Guo, X.; Liu, L.; Zhai, H.; Meng, Q.; Shi, Z.; Tai, X. Two d^{10} luminescent metal–organic frameworks as dual functional luminescent sensors for (Fe^{3+},Cu^{2+}) and 2,4,6-trinitrophenol (TNP) with high selectivity and sensitivity. *Rsc Adv.* **2020**, *10*, 4817-4824.
59. Wang, Q.; Dong, J.; Li, Z.; Wang, X.; He, Y.; Chen, B.; Zhao, D. Dual-Emitting Mixed-Lanthanide Metal-Organic Framework for Ratiometric and Quantitative Visual Detection of 2,6-Pyridine Dicarboxylic Acid. *Inorg. Chem.* **2023**, *62*, 14439-14447.
60. Pan, J.; Lu, J.; Shang, Y.; Li, Y.; Yan, B. Tb(iii)-functionalized MOF hybridized bis-crosslinked networked hydrogel luminescent films for arginine and dopamine hydrochloride sensing and anticounterfeiting. *J. Mater. Chem. C* **2025**, *13*, 1198-1206.
61. Yu, H.; Yang, X.; Lv, X.; Huang, X. Construction of a 12-metal Zn(II)-Nd(III) nanocluster for ratiometric fluorescence detection of inflammatory marker neopterin. *J. Rare Earth* **2025**, *43*, 270-275.
62. Sun, Y.; Wang, X.; Liu, S.; Yang, X.; Ren, X.; Liu, W.; Liu, W. Functional Construction of a Novel Lanthanide MOF for Efficient Ratio Luminescence Detection of Ethanol Vapor. *Adv. Opt. Mater.* **2024**, *12*, 2400692.
63. Dong, Y. L.; Song, W.; Hu, J.; Ren, C. L. A Facile Solid-Phase Synthesis of Scandium-Modified Carbon Dots for Fluorescent Sensing of Cu^{2+}. *Chemosensors* **2025**, *13*, 430.
64. Kotnana, G.; Hong, S. G. Recent Progress on Rare Earth Orthoferrites for Gas-Sensing Applications. *Chemosensors* **2025**, *13*, 156.

 doi:10.20944/preprints202605.1703.v1

65. Xia, Y. P.; Zhu, X. S.; Yang, H.; Zhou, F.; Zhu, R. X.; Zhang, Y. T.; Zheng, S. R.; Zheng, Z. P. Synthesis, crystal structure, spectroscopic and theoretical studies of a new fluorescent heterocyclic compound containing diketopyrrolopyrrole (DPP) moiety. *J. Mol. Struct.* **2024**, *1318*, 139334.
66. Zeng, W. L.; Wang, X.; Zhang, Y. J. Synthesis, Crystal Structures, and Density Functional Theory Studies of Two Salt Cocrystals Containing Meldrum's Acid Group. *Acs Omega* **2022**, *7*, 25132-25139.
67. Stephens, P. J.; Devlin, F. J.; Chabalowski, C. F.; Frisch, M. J. Ab Initio Calculation of Vibrational Absorption and Circular Dichroism Spectra Using Density Functional Force Fields. *J. Phys. Chem.* **1994**, *98*, 11623-11627.
68. Xi-Shi, T.; Li-Hua, W.; Al-Resayes, S. I.; Azam, M. A novel Ca(II) coordination polymer with 3-(3-carboxyphenyl)-isonicotinic acid: design, DFT analysis, and catalytic efficiency. *BMC Chem.* **2026**, *20*, 55.
69. Sui, B.-L.; Wang, L.-H.; Tai, X.-S.; Al-Resayes, S. I.; Azam, M.; Wang, A.-L. Synthesis, structural characterization, DFT calculation, and antitumor activity of a new Co(II) complex based on 2-((2′-Carboxybenzyl)oxy)benzoic acid and 2,2′-bipyridine ligands. *BMC Chem.* **2026**, *20*, 51.
70. Zeng, W. L.; Yue, D. Y.; Wang, X.; Kong, X. J. Vibrational spectroscopy, DFT calculations, MEP, NBO, NLO and Hirshfeld surface studies of a new Meldrum's acid derivative containing 2-hydroxyphenylamino moiety. *J. Mol. Struct.* **2025**, *1341*, 142675.
71. Ding, R.; Liu, J. J.; Meng, Q. G.; Wang, T.; Zhang, X. M. Dual-functional flexible cationic porphyrin-based covalent organic frameworks for selective adsorption and sensitive detection of Cr(VI). *Sep. Purif. Technol.* **2025**, *359*, 130544.
72. Xi-Shi, T.; Li-Hua, W.; Al-Resayes, S. I.; Azam, M. Design, Structural Characterization, and Fluorescence Behavior of a New Centrosymmetric Dinuclear Cd(II) Complex With 2-Formylphenoxyacetic Acid and 1,10-Phenanthroline. *J. Spectrosc.* **2026**, *2026*, 9957210.
73. Wang, L. H.; Yan, X. H.; Tai, X. S.; Al-Resayes, S. I.; Azam, M. Design and Structural Investigation, Hirschfeld Surface Analysis, and Photoluminescent Behavior of a Cd(II) Coordination Polymer With 4-Acetylphenoxyacetic Acid Ligand. *J. Spectrosc.* **2026**, *2026*, 3903190.
74. Xia, Y. P.; Huang, Y. X.; Zhou, F.; Huang, Z. R.; Yan, J. W.; Lv, J. H.; Tang, F. F. Synthesis, crystal structure, spectroscopic, DFT calculation and GCMC simulation studies of a new Cu(II) metal-organic framework based on 5-(1H-1,2,4-triazol-1-yl)isophthalic acid. *Polyhedron* **2025**, *281*, 117748.
75. Wang, K.; Zhu, Y. L.; Zheng, T. F.; Xie, X.; Chen, J. L.; Wu, Y. Q.; Liu, S. J.; Wen, H. R. Highly pH-Responsive Sensor Based on a EuIII Metal-Organic Framework with Efficient Recognition of Arginine and Lysine in Living Cells. *Anal. Chem.* **2023**, *95*, 4992-4999.
76. Della Pelle, F.; Angelini, C.; Sergi, M.; Del Carlo, M.; Pepe, A.; Compagnone, D. Nano carbon black-based screen printed sensor for carbofuran, isoprocarb, carbaryl and fenobucarb detection: application to grain samples. *Talanta* **2018**, *186*, 389-396.
77. Gao, R. R.; Qiu, Q.; Dong, W. Visual Monitoring of Levofloxacin in Biofluids by Europium(III)-Functionalized Mesoporous Silica Nanoparticles. *Acs Appl. Nano Mater.* **2022**, *5*, 5631-5639.
78. Su, Y. Q.; Fu, L. S.; Cui, G. H. Two chemically robust Cd(ii)-frameworks for efficient sensing of levofloxacin, benzaldehyde, and Fe^{3+} ions. *Dalton Trans.* **2021**, *50*, 15743-15753.
79. Zeng, W. L.; Yue, D. Y.; Wang, X.; Li, H. Y.; Kong, X. J. Synthesis, structural, spectroscopic investigation, Hirshfeld surface analysis and DFT calculation of a new spiro compound including 4-nitroaniline moiety. *J. Mol. Struct.* **2025**, *1322*, 140371.